A detailed comparison of MYD11 and MYD21 land surface temperature products in mainland China

7 authors, including:

Rui Yao
Wuhan University
40 PUBLICATIONS   **2,010** CITATIONS

SEE PROFILE

li Junli
Anhui Agricultural University (AHAU)
23 PUBLICATIONS   **390** CITATIONS

SEE PROFILE

Some of the authors of this publication are also working on these related projects:

Project   estimating air temperature using satellite data View project

Project   urbanization effects on urban heat island and vegetation View project

A detailed comparison of MYD11 and MYD21 land surface temperature products in mainland China

Rui Yao, Lunche Wang, Shaoqiang Wang, Lizhe Wang, Jing Wei, Junli Li & Deqing Yu

Published online: 06 Jan 2020.

Submit your article to this journal 🖉

View related articles 🔍

View Crossmark data ✓

Check for updates

A detailed comparison of MYD11 and MYD21 land surface temperature products in mainland China

Rui Yao[a,b], Lunche Wang [a,b], Shaoqiang Wang[a,b], Lizhe Wang[c,d], Jing Wei[e,f], Junli Li[g] and Deqing Yu[h]

[a]Hunan Key Laboratory of Remote Sensing of Ecological Environment in Dongting Lake Area, School of Geography and Information Engineering, China University of Geosciences, Wuhan, People's Republic of China; [b]Hubei Key Laboratory of Critical Zone Evolution, School of Geography and Information Engineering, China University of Geosciences, Wuhan, People's Republic of China; [c]Faculty of Computer Science, China University of Geosciences, Wuhan, People's Republic of China; [d]Hubei Key Laboratory of Intelligent Geo-Information Processing, China University of Geosciences, Wuhan, People's Republic of China; [e]State Key Laboratory of Remote Sensing Science, College of Global Change and Earth System Science, Beijing Normal University, Beijing, People's Republic of China; [f]Department of Atmospheric and Oceanic Science, Earth System Science Interdisciplinary Center, University of Maryland, College Park, MD, USA; [g]School of Resources and Environment, Anhui Agricultural University, Hefei, Anhui, People's Republic of China; [h]Hunan Key Laboratory of remote sensing of ecological environment in Dongting Lake Area, Hunan Natural Resources Affairs Center, Changsha, People's Republic of China

ABSTRACT

Land surface temperature (LST) is a key parameter in land surface system. The National Aeronautics and Space Administration (NASA) recently released new Moderate Resolution Imaging Spectroradiometer (MODIS) LST products (MOD21 and MYD21). Here, we conducted a detailed comparison between the MYD11 and MYD21 LST data in mainland China. The LSTs of MYD21 were approximately 1°C higher than those of MYD11 averaged for mainland China, as MYD21 corrected the cold bias of MYD11. The proportions of the valid value of MYD21 were generally lower than those of MYD11 because the cloud removal method of MYD21 was stricter than that of MYD11. Furthermore, the outliers were less significant in MYD11 than in MYD21 because the outliers in MYD11 were removed using temporal constraints on LST. The outliers in MYD21A2 resulted in a difference of greater than 3°C in average seasonal surface urban heat island intensity (SUHII) between MYD11A2 and MYD21A2. Finally, using MYD11 may underestimate the slope of long-term trends of SUHII. MYD21 LST data may have some uncertainties in urban areas. This study provided a reference for users for selecting LST products and for data producers to further improve MODIS LST products.

1. Introduction

Land surface temperature (LST) is a key variable in various fields (Phan and Kappas 2018; Weng 2009). For example, LST can be employed to investigate the surface urban heat island (SUHI) effect, agricultural drought and climate change (Yao et al. 2019; Zhou and Wang 2016), estimate air temperature and evapotranspiration (Bhattarai et al. 2019; Lu et al. 2018) and analyze land cover change and urbanization (Huang et al. 2018; Hulley, Veraverbeke, and Hook 2014). Remote

sensing is the most effective approach for obtaining LST information over a large area. One important LST product is the National Aeronautics and Space Administration (NASA) Moderate Resolution Imaging Spectroradiometer (MODIS) LST product. It is freely available and has relatively high accuracy, global coverage, acceptable spatial resolution (1 km) and high temporal resolution (four times a day for two satellites). Therefore, these products have been widely used in previous studies across many fields (Bhattarai et al. 2019; Huang et al. 2018; Hulley, Veraverbeke, and Hook 2014; Wan 2008; Xu et al. 2018; Zhou and Wang 2016; Zhou et al. 2018).

The traditional and widely used MODIS LST products are the MxD11 (MOD11 and MYD11) LST and emissivity products. A split-window algorithm is used to retrieve LST at a 1 km spatial resolution (Wan 2008, 2014; Wan and Dozier 1996). In the second half of 2018, NASA distributed the MODIS MxD21 (MOD21 and MYD21) LST and emissivity products. The MxD21 products use an improved water vapor scaling method to remove the atmospheric effects. The LST and emissivity at a 1 km spatial resolution are retrieved employing a temperature emissivity separation (TES) method (Hulley, Malakar, and Freepartner 2016a). The MxD21 products were found to have some advantages compared with the MxD11 products (Coll et al. 2016; Ermida et al. 2014; Hulley, Veraverbeke, and Hook 2014; Hulley et al. 2018; Malakar and Hulley 2016; Hulley, Malakar, and Freepartner 2016a; Hulley et al. 2016b). First, Hulley, Malakar, and Freepartner (2016a) used a radiance-based method to validate the accuracies of the MYD21 and MYD11 products at six bare sites, two water sites and two vegetated sites. Compared with the MYD11 products, the MYD21 products have significantly higher accuracy over barren surfaces (MYD21 product: RMSE ranges from 0.5–1.5°C; MYD11 product: RMSE ranges from 1.1–4.1°C) and comparable accuracy over water and vegetated surfaces (MYD21 product: RMSE ranges from 0.9–1.3°C; MYD11 product: RMSE ranges from 0.5–1.5°C). Second, the MxD21 data can be used to detect land cover changes, whereas MxD11 can not because MxD11 assigned a fixed emissivity value according to land cover type (Hulley, Veraverbeke, and Hook 2014). Third, Hulley et al. (2018) showed that the LST of the MYD21 product was highly consistent with the Visible Infrared Imaging Radiometer Suite (VIIRS) VNP21 TES product, with an RMSE less than 1°C. However, there were significant differences in LST between the MYD11 and VIIRS VLSTO split-window products, with an RMSE ranging from 1.2–3.0°C. Therefore, the continuity and consistency between the MYD21 and VNP21 LST products will help us better understand the Earth system dynamics (Hulley et al. 2018).

Overall, previous studies have compared the accuracy of the MYD11 and MYD21 products (Coll et al. 2016; Ermida et al. 2014; Malakar and Hulley 2016) and analyzed the consistency of LST products across sensors (Hulley et al. 2018; Islam et al. 2017). However, to our knowledge, few studies have compared other information (e.g. the amount of extreme and missing values) and practical applications in terms of analyzing the SUHI effect. To fill these research gaps, this study aims to compare (1) the differences in LST between the daily MYD11A1 and MYD21A1D/MYD21A1N LST products during 2014–2016 and between the 8-day composite MYD11A2 and MYD21A2 LST products from 2003–2018 in mainland China, (2) the proportions of missing values between the MYD11 and MYD21 products, (3) the extreme values between the MYD11 and MYD21 products, and (4) the SUHI effect revealed by the MYD11A2 and MYD21A2 products in 31 major cities in mainland China.

2. Materials and methods

2.1. Study area

Mainland China is actively studied in terms of its climate and SUHI because the country has undergone rapid urbanization and is sensitive to climate change (Ding et al. 2007; Xu et al. 2019; Yao et al. 2018a; Niu et al. 2019; Zhou et al. 2018; Wei et al. 2019a; Wei et al. 2019b). Therefore, mainland China was chosen as the study area (Figure 1). Climate, elevation and land cover differ greatly across mainland China: southeastern China has a hot-humid climate, whereas northwestern China has a
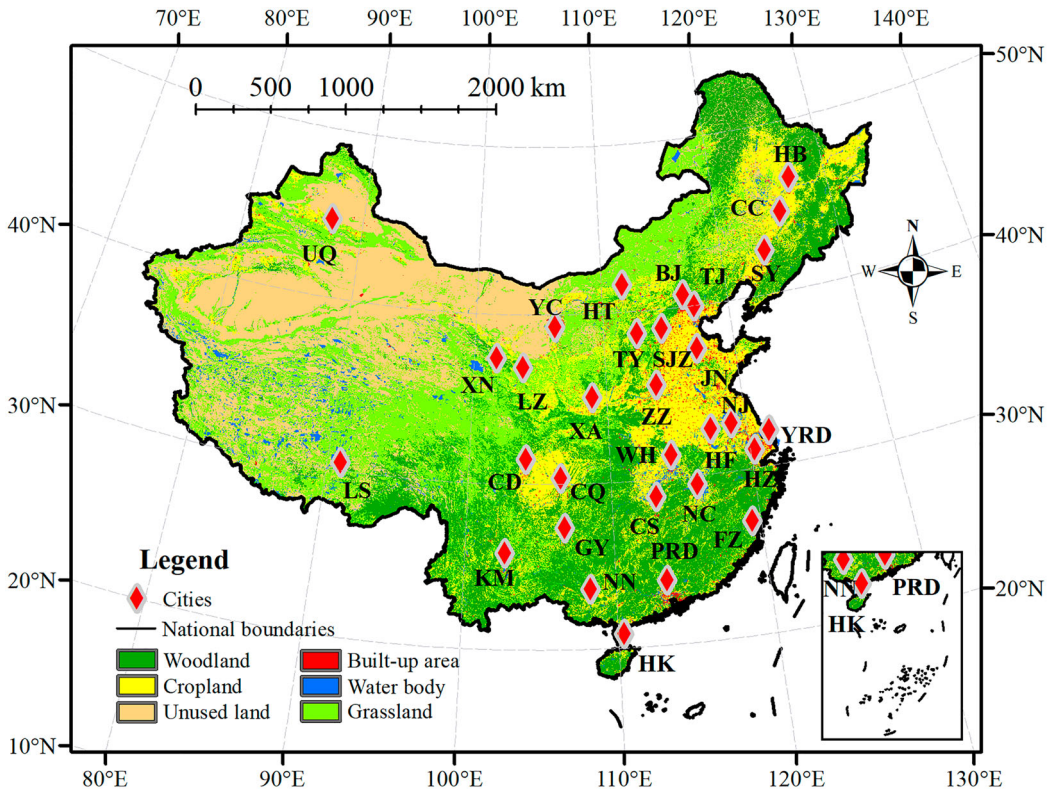
Figure 1. Study area and locations of the 31 major cities of this study. The land cover map is China's Land Use/Cover Dataset (CLUD) in 2015. The 31 selected cities were Beijing (BJ), Changchun (CC), Guiyang (GY), Urumqi (UQ), Harbin (HB), Shenyang (SY), Lhasa (LS), Hohhot (HT), Yinchuan (YC), Shijiazhuang (SJZ), Taiyuan (TY), Jinan (JN), Xining (XN), Zhengzhou (ZZ), Nanjing (NJ), Hefei (HF), Fuzhou (FZ), Hangzhou (HZ), Wuhan (WH), Chengdu (CD), Haikou (HK), Chongqing (CQ), Nanchang (NC), Changsha (CS), Kunming (KM), Nanning (NN), Lanzhou (LZ), Tianjin (TJ), Xi'an (XA), Pearl River Delta urban agglomeration (PRD) and Yangtze River Delta urban agglomeration (YRD).

cold-dry climate. Additionally, the elevation gradually decreases from western China (e.g. the Qinghai-Tibetan Plateau) to eastern China; furthermore, northwestern China has a large amount of barren surfaces (e.g. the Tarim Basin) due to its dry climate, whereas southeastern China generally has vegetated surfaces (e.g. woodland and cropland) due to its humid climate (Figure 1). In addition, the SUHI effect was analyzed in 31 major cities, including 3 municipalities, 26 provincial capitals and 2 urban agglomerations (Figure 1).

2.2. Data and preprocessing

Only three types of MxD21 LST products are available online: (1) the MxD21 1 km resolution swath product, (2) MxD21A1D and MxD21A1N 1 km resolution daily product, and (3) MxD21A2 1 km resolution 8-day composite product. The 1 km resolution daily and 8-day composite LST products

Table 1. Moderate resolution imaging spectroradiometer (MODIS) land surface temperature (LST) products utilized in this study.

LST product	Spatial resolution	Temporal resolution	Time period in this study	Collection
MYD11A1	1 km	Daily	2014–2016	6
MYD21A1D/MYD21A1N	1 km	Daily	2014–2016	6
MYD11A2	1 km	8 day	2003–2018	6
MYD21A2	1 km	8 day	2003–2018	6

from the Aqua satellite were used in this study (Table 1). The accuracy of MxD11 LST data has been widely validated by previous studies (Wan 2008; Duan et al. 2018, 2019). For example, Duan et al. (2018) used a radiance-based method to validate LST over 38 validation sites. The results showed that the RMSEs were less than 1 K for Collection 6 MxD11 LST for most sites. MOD21 LST products from the Terra satellite were not used, because these products are not available from 2009 to the present due to an optical crosstalk issue in the infrared bands (band 27–30) (Hulley 2019). Note that the MYD11A1, MYD11A2 and MYD21A2 products contain both daytime and nighttime LST, whereas the MYD21A1D product includes only daytime LST and the MYD21A1N product includes only nighttime LST. The MODIS reprojection tool (MRT) was utilized to re-project and mosaic the original LST products.

The land use/land cover information in 2000 and 2015 were derived from China's Land Use/ Cover Datasets (CLUDs) of 30 m spatial resolution (Kuang et al. 2016; Liu et al. 2014). They have 25 land cover types, and the overall accuracies are greater than 90%. To match the LST data, the 30 m resolution CLUDs were converted into (1) proportional land cover data with 1 km resolution, where the proportions of each land cover type within each 1 km resolution pixel were calculated using the original 30 m resolution CLUDs, and (2) land cover type data with 1 km resolution, where the land cover type of a pixel was classified as the land cover type with the highest proportion. Advanced Spaceborne Thermal Emission and Reflection Radiometer (ASTER) digital elevation model (DEM) data with a 30 m spatial resolution were used in this study and aggregated to a resolution of 1 km.

2.3. Methods

MODIS LST data include quality information stored in quality control (QC) layer. The QC values range from 0 to 3. The QC value of 0 represents the best data and 3 represents the worst data (Wan 2013; Hulley et al. 2016b). LST data with all QC values were used in the present study. Thus, all valid LST data were used in the later analyses. The experiments of this study included four sections. First, the average differences in LST between the daily MYD11A1 and MYD21A1D/ MYD21A1N products for the period of 2014–2016 and between the 8-day MYD11A2 and MYD21A2 products from 2003–2018 were analyzed for each pixel in mainland China (Section 3.1). There were many missing values in the LST products due to cloud contamination and other factors. For each pixel, the difference in LST was calculated only when both the MYD11 and MYD21 products had no missing values. Second, the proportions of valid values of the MYD11A1 and MYD21A1 products for the period of 2014–2016 and of MYD11A2 and MYD21A2 products during 2003–2018 were calculated for each pixel in mainland China (Section 3.2). Third, for each daily data during 2014–2016 and 8-day composite LST data from 2003–2018, we calculated four values as follows: (1) the LST higher than 99.995% of LST in mainland China (defined as extremely high LST in this study), (2) the LST lower than 99.995% of LST in mainland China (defined as extremely low LST in this study), (3) the highest LST in mainland China, and (4) the lowest LST in mainland China (Section 3.3).

The SUHI effect was analyzed using MYD11A2 and MYD21A2 data in 31 major cities in mainland China (Section 3.4). The spatial extents of urban areas in 2000 and 2015 in the 31 selected cities were first extracted from the CLUDs. The spatial extents of urban areas in 2000 were defined as old urban areas (OUAs). In addition, the OUAs were excluded from the spatial extents of urban areas in 2015, and the remaining parts were defined as urbanizing areas (UAs). Next, 10–30 km buffers were generated around the urban areas in 2015 (Yao et al. 2019), and pixels in the 10–30 km buffers that met one of the following requirements were excluded because these pixels affect the estimation of the SUHI effect: (1) pixels with a water body proportion greater than 0%; (2) pixels with a built-up area proportion greater than 0%; and (3) pixels with an elevation outside the range of the average elevation of urban areas ± 50 m (Yao et al. 2017b; Zhou et al. 2016; Wu et al. 2019). The remaining parts of the 10–30 km buffers were defined as rural areas. The buffer range of 10–30 km was selected,

because: (1) the footprint of the SUHI covers not only the urban area but also the nearby area around the urban area with a distance less than 10 km (Han and Xu 2013; Zhang et al. 2004; Zhou et al. 2015), and (2) if the selected rural areas are far from the urban areas, the estimation of the SUHI effect will be influenced by climate variability (Yao et al. 2017a; Zhou et al. 2015). Subsequently, the SUHI intensity (SUHII), a widely used indicator of SUHI, was calculated using Equation (1):

$$SUHII = LST_{urban} - LST_{rural} \tag{1}$$

where LST_{urban} and LST_{rural} are the spatial average LSTs of urban and rural areas, respectively. The MYD11A2 and MYD21A2 LST products were averaged into summer (defined as from June to August), winter (defined as from December to February) and annual mean and used to analyze the SUHI effect. The SUHII in 2015 was first determined, and the long-term trends of the SUHII during 2003–2018 were then analyzed utilizing linear regression analysis.

3. Results and discussion

3.1. LST differences between MYD11 and MYD21 products

The spatial distributions of the differences in LST between the MYD11 and MYD21 products are shown in Figure 2. The LST of the MYD21 products was higher than that of the MYD11 products in most areas in mainland China, except for the daytime LST in the northern Qinghai-Tibetan Plateau. The LSTs of MYD21A1 were 1.00 and 0.65°C higher than those of MYD11A1 during the daytime and nighttime, respectively, which are average for mainland China. The LSTs of MYD21A2 were, on average, 0.94 and 0.94°C higher than those of MYD11A2 during the daytime and nighttime, respectively.
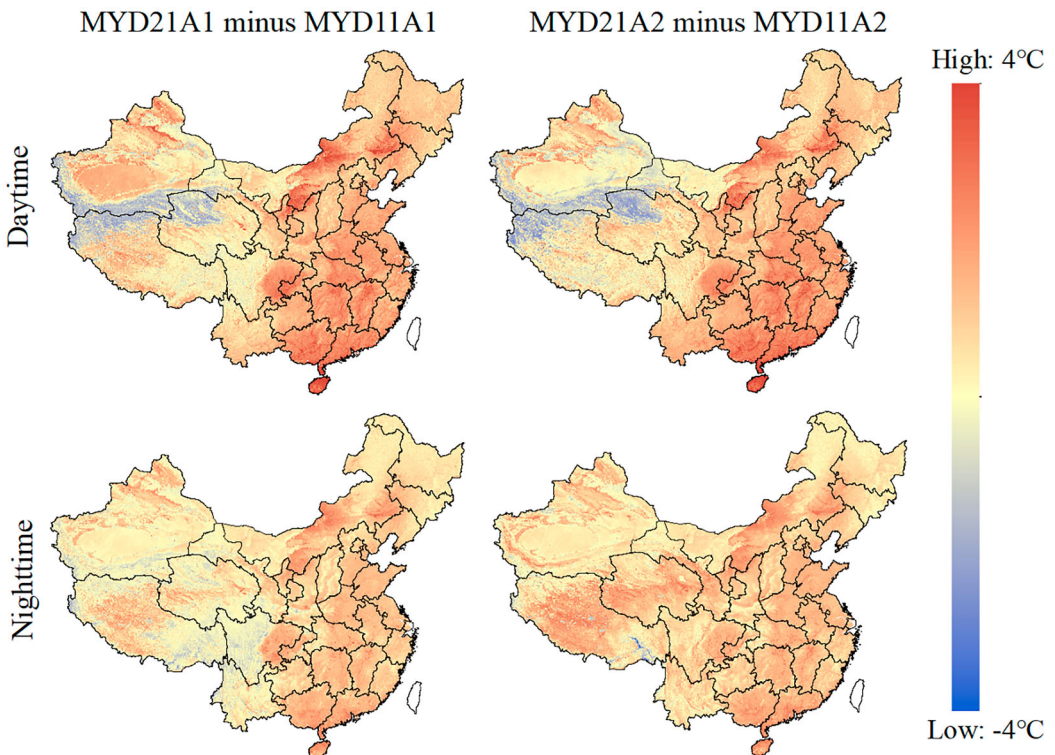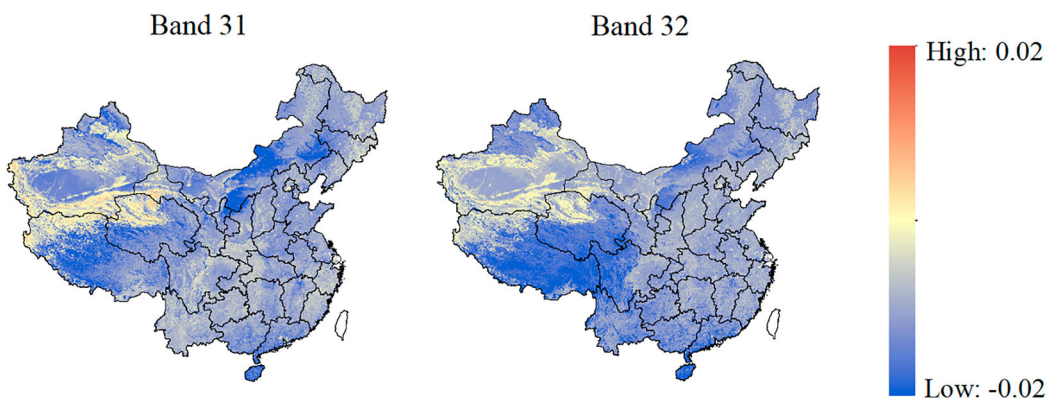

Figure 2. Differences in Land surface temperature (LST) between the MYD11A1 and MYD21A1D/MYD21A1N products averaged for the period of 2014–2016 and between the MYD11A2 and MYD21A2 products averaged from 2003–2018.

These two LST products use different algorithms to retrieve the LST. MYD11 uses a split-window algorithm to retrieve LST, whereas the MYD21 product uses a TES algorithm (Malakar and Hulley 2016; Wan 1999; Wan and Dozier 1996; Hulley, Malakar, and Freepartner 2016a). The major difference between these two products is that MYD11 assigns fixed emissivity values according to land cover information, whereas MYD21 dynamically retrieves emissivity (Hulley, Malakar, and Freepartner 2016a). Compared with MYD11 products, MYD21 can avoid emissivity errors originating from three main sources: (1) classification errors in land cover type; (2) emissivity errors within land cover type (e.g, bare land); and (3) dynamic changes in land cover type (Hulley, Malakar, and Freepartner 2016a). The higher LST of MYD21 than that of MYD11 in arid areas is because MYD21 corrects the cold bias of MYD11 in arid areas. The cold bias of MYD11 in arid areas can be explained by the fact that MYD11 assigns fixed emissivity values according to land cover information. This method leads to higher assigned emissivity than real emissivity and lower retrieved LST than real LST over bare sites where the surface composition varies greatly (Hulley, Malakar, and Freepartner 2016a). In addition, the higher LST of MYD21 than that of MYD11 in vegetated areas and water surfaces can be explained by the fact that MYD21 slightly overestimates the LST, and MYD11 slightly underestimates the LST in vegetated areas and water surfaces (Hulley, Malakar, and Freepartner 2016a). In addition, the lower LST of MYD21 than that of MYD11 in the northern Qinghai-Tibetan Plateau can primarily be attributed to higher emissivity of MYD21 products than that of MYD11 (Figure 3). This is because these two products use different methods to obtain the emissivity of the land surface. MYD11 may cause some uncertainties because the emissivities of some land cover types (e.g. barren surface such as the northern Qinghai-Tibetan Plateau) are not fixed and have a certain range (Hulley, Malakar, and Freepartner 2016a).

The differences in LST between the MYD11A1 and MYD21A1 products over different land cover types are shown in Table 2. The LST of MYD21A1 was higher than that of MYD11A1 over all land cover types. The differences in LST were highest in built-up areas because there were many extremely high LST in MYD21A1, especially in built-up areas. Further analysis showed that the daytime (night-time) LST of MYD21A1 was 5°C higher than MYD11A1 over 0.87% (0.28%) of built-up areas, whereas this proportion was 0.06% (0.01%) on average for the other land cover types. The differences in LST were the lowest in unused land, because the LST of MYD21A1 was equal to or lower than that of MYD11A1 in parts of the Qinghai-Tibetan Plateau.

3.2. The proportions of valid values of LST products

The proportions of valid values of LST products are shown in Figure 4 and Table 3. Spatially, the proportions of valid values of LST products were generally higher in northwestern China than in


Figure 3. Emissivity differences between the MYD11A2 and MYD21A2 products averaged for the period of 2014–2016.

Table 2. Differences in LST (℃) between the MYD11A1 and MYD21A1D/MYD21A1N products averaged for the period of 2014–2016 over different land cover types (using CLUD in 2015).

	Woodland	Cropland	Unused land	Built-up area	Water body	Grassland
Daytime	1.24	1.71	0.43	1.86	0.67	0.74
Nighttime	0.63	1.13	0.37	1.26	0.77	0.52
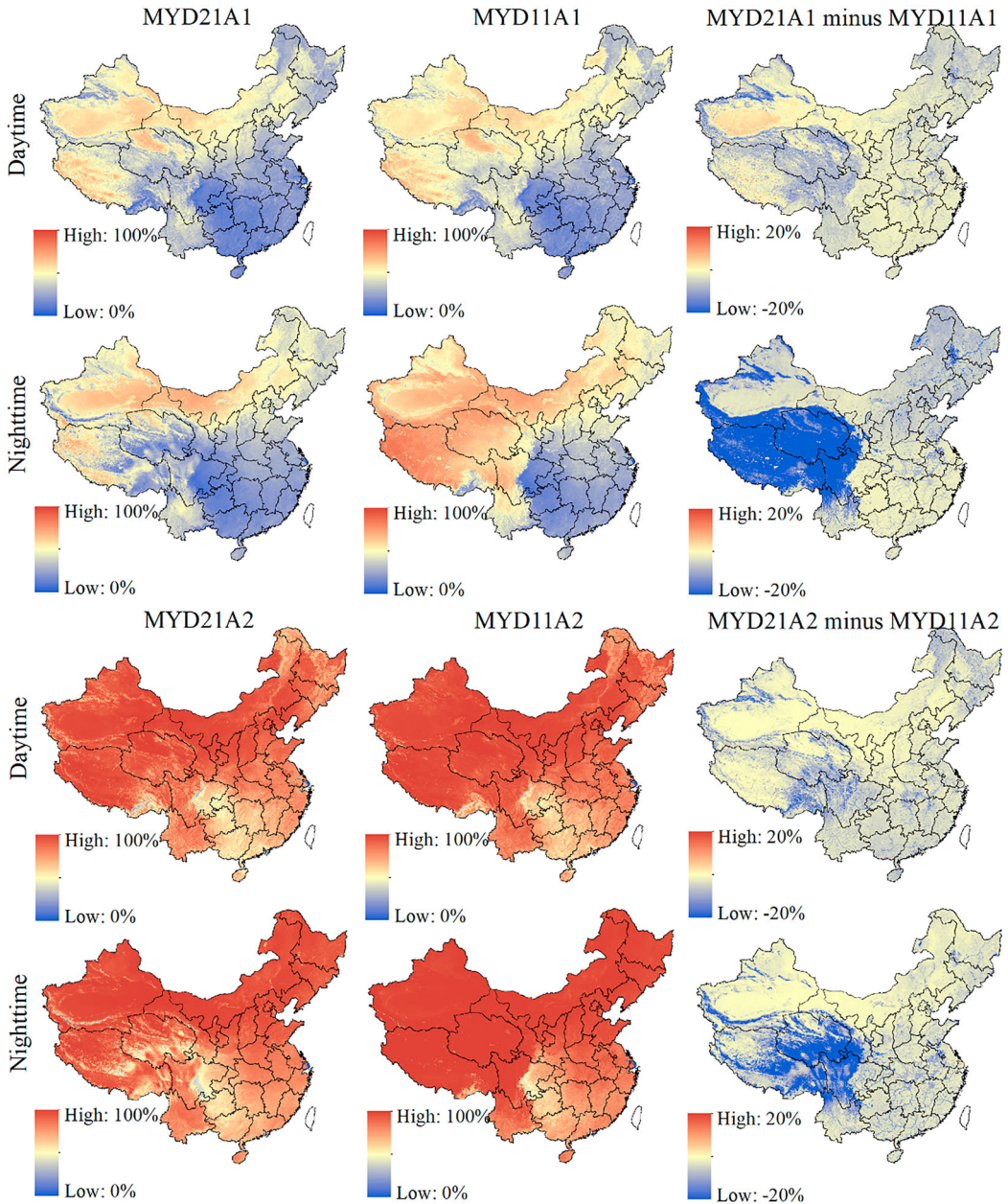
Figure 4. Proportions of valid values of MYD11A1 and MYD21A1 products and their differences.

southeastern China. The lowest proportion of valid values was found in the Sichuan Basin. These results are because southeastern China is characterized by a humid and cloudy climate, whereas northwestern China has a dry and sunny climate. Signals from land surfaces cannot penetrate clouds;

Table 3. The proportion of valid pixels of LST products averaged for mainland China.

	MYD11A1	MYD21A1	MYD11A2	MYD21A2
Daytime	41.0%	37.3%	88.8%	85.1%
Nighttime	50.9%	38.8%	92.6%	85.6%

therefore, LST is retrieved only when there are clear-sky conditions. In addition, the proportions of valid values of the 8-day composite MYD11A2 and MYD21A2 products were much higher than that obtained for the daily MYD11A1 and MYD21A1 products (Figure 4 and Table 3). The proportions of valid values of 8-day composite LST products were all higher than 85% averaged for mainland China, while the proportions of valid values of daily LST products were all lower than 51% (Table 3). These results are because the MYD11A2 and MYD21A2 products average the daily LST products into eight days, and the invalid pixels were not processed in this procedure (Wan 2013; Hulley et al. 2016b). Finally, the proportions of the valid values of the MYD11A1 product were 41.0% and 50.9% for the daytime and nighttime LST, respectively. These values were higher than those for the MYD21A1 product (Table 3). The proportions of valid values of the MYD21 products were lower than those of the MYD11 products for most regions in mainland China, especially in the Qinghai-Tibetan Plateau. The reason for these phenomena is that these two MODIS LST products use different methods to remove the effects of clouds. The MYD21A1 product excludes the pixels with a confidence of clear-sky conditions ≤ 95% using the MOD35 cloud mask product. However, the MYD11A1 product uses more complicated methods: (1) excluding pixels with a confidence of clear-sky conditions ≤ 95% over land with an elevation ≤ 2000 m, (2) excluding pixels with a confidence of clear-sky conditions ≤ 66% over land with an elevation > 2000 m, (3) excluding pixels with a confidence of clear-sky conditions ≤ 66% over lakes, and (4) using temporal constraints on LSTs in 32 days (Wan 2008, 2013). Therefore, the proportions of valid values of the MYD21 products were greater than those of the MYD11 products, especially in the Qinghai-Tibetan Plateau.

3.3. Extreme values in LST products

The extreme LSTs were more significant in the MYD21 products than in the MYD11 products (Figures 5 and 6). The extremely high LST in the MYD21A1 products exceeded 100°C on certain days. The highest LST in MYD21A1 on many days was as high as 100°C, and on certain days it exceeded 500°C (not shown in Figures 5 and 6). Although MYD21A2 is an 8-day average product, the extremely high LST in MYD21A2 reached up to 100°C on certain days, and the highest LST in MYD21A2 easily exceeded 100°C (Figure 6). Comparatively, the extremely high and the highest LSTs in the MYD11 product in mainland China were stable across days and showed a clear seasonal cycle. Further analysis showed that the extremely high LST was generally accompanied by extremely low emissivity (not shown). Therefore, the extremely high LST in the MYD21 products may be attributed to the incorrect retrieval of emissivity (Hulley, Malakar, and Freepartner 2016a). In addition, the lowest and extremely low LSTs in mainland China in the MYD21 products were relatively close to those of the MYD11 products, and significant differences were generally found in winter. The extremely low LSTs can generally be attributed to undetected clouds (Xu et al. 2018). The above results clearly indicated that the extreme LST was more significant in the MYD21 products than in the MYD11 products. This phenomenon occurred because the MYD11 products use temporal constraints on LST to remove outliers (Wan 2008, 2013), whereas the MYD21 products do not. Specifically, the extreme LSTs in MYD11 were removed using the following four steps. First, the LSTs that were higher or lower than the highest LST in 32 days by more than four times the ΔT (a variable determined by land cover) were removed. Second, the LSTs that were higher or lower than the highest LST in 16 days by more than three times the ΔT were removed. Third, the LSTs that were higher or lower than the highest LST in 8 days by more than two times the ΔT were removed. Fourth, the LSTs that were higher or lower than the 8-day average LST by more
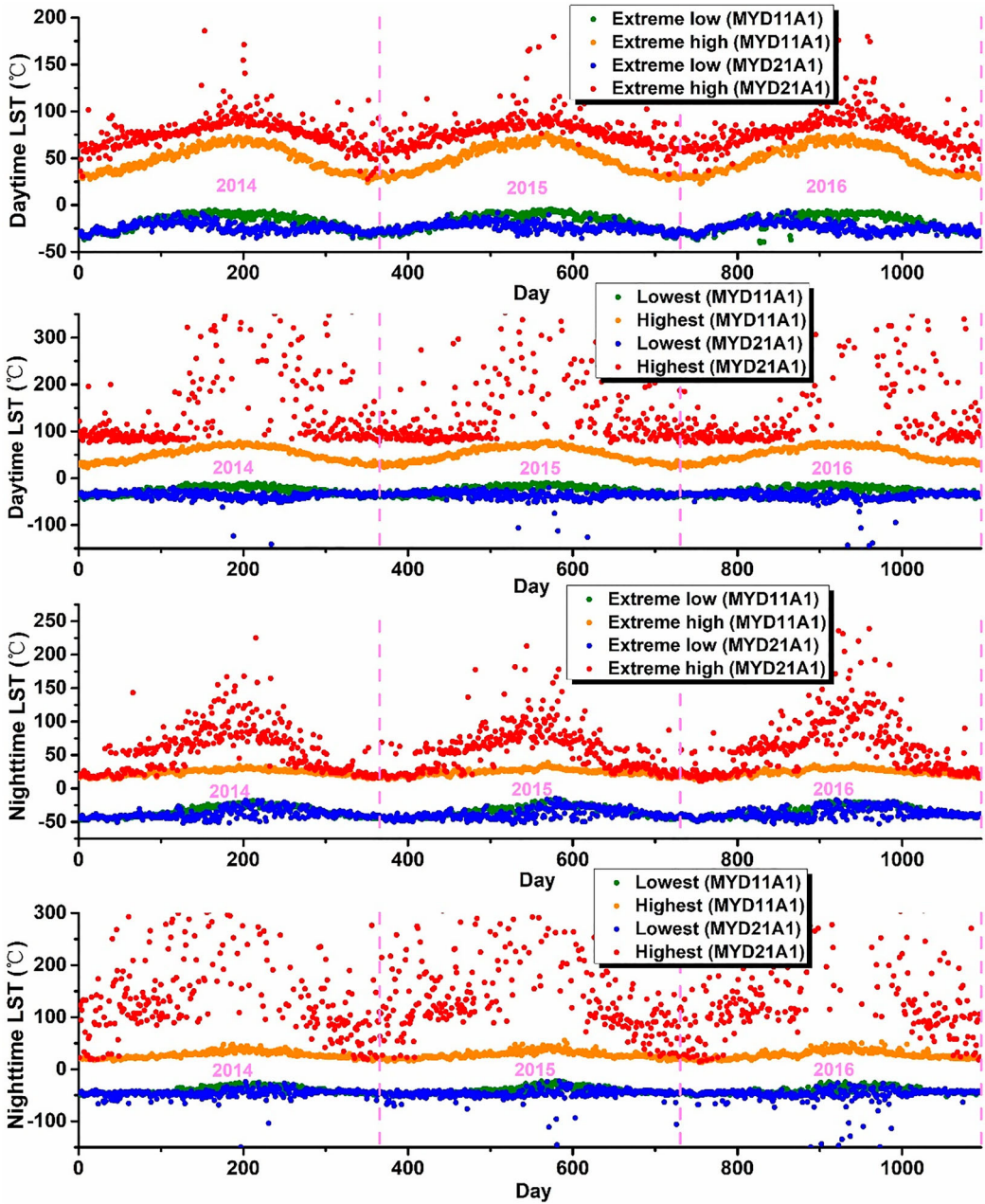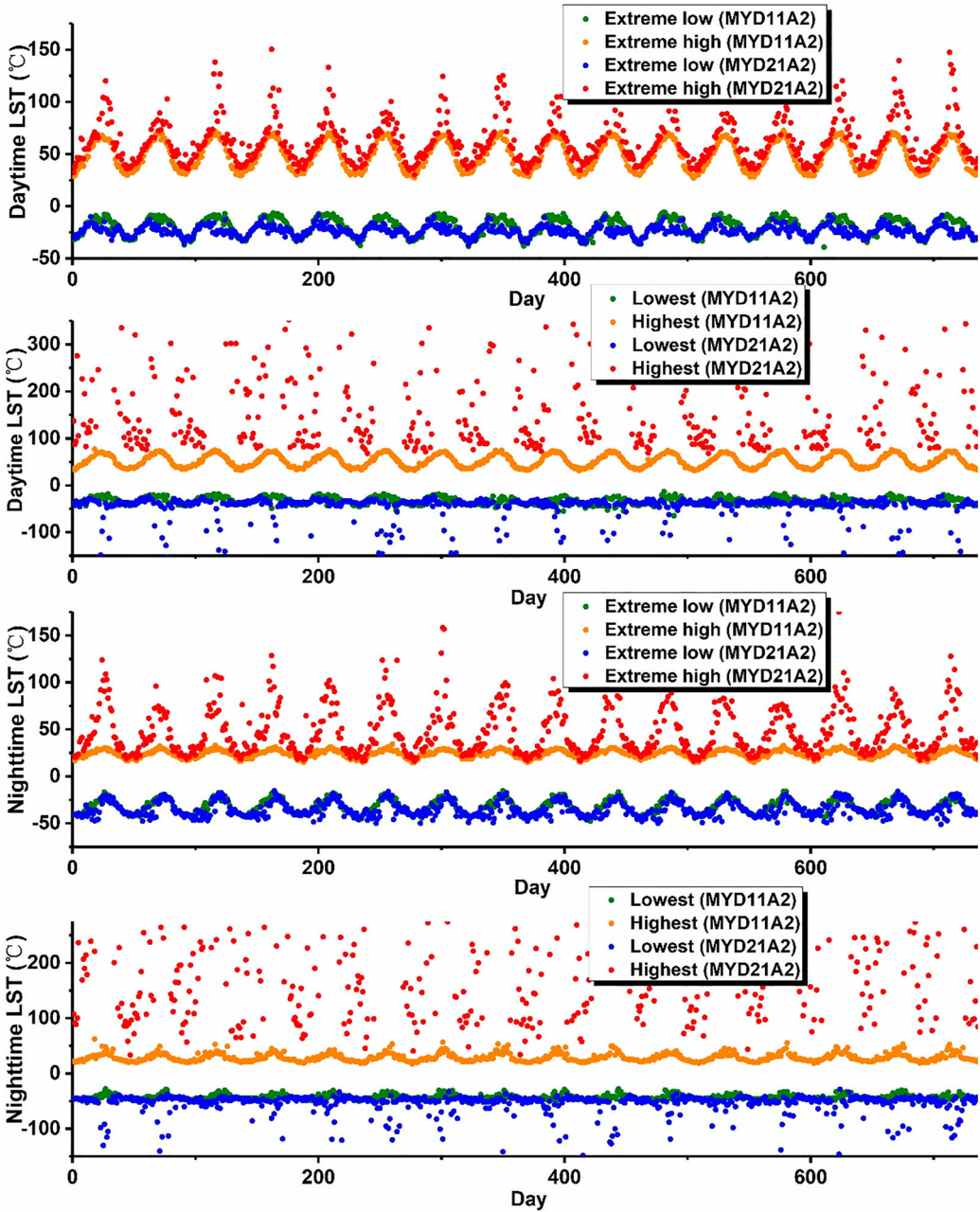
Figure 5. The extremely high and low LST, and the highest and lowest LST in mainland China in the MYD11A1 and MYD21A1 products during 2014–2016.

than the ΔT were removed (Wan 2008). Overall, the MYD21 products have many outliers, which may inhibit their practical applications.

### 3.4. SUHI effect revealed by LST products

The spatial distribution of the SUHII in mainland China in 2015 that was revealed by MYD11A2 was similar to that revealed by the MYD21A2 product (Figure 7). The daytime SUHII differed

Figure 6. The extremely high and low LST, and the highest and lowest LST in mainland China in the MYD11A2 and MYD21A2 products during 2003–2018.

substantially across cities and seasons, with higher daytime SUHII values found in southeastern China and during summer. These results were similar to Yao et al. (2017b) and Zhou et al. (2014). Daytime SUHII is strongly related to background vegetation conditions, as vegetation transpiration can reduce LST during the daytime. Rural vegetation in southeastern cities is usually more abundant than in northwestern cities because southeastern cities have a more humid climate, which is more suitable for vegetation growth. In addition, the amount of rural vegetation is commonly

higher in summer than in winter and higher than the annual mean. A large amount of rural vegetation can increase the differences in vegetation between urban and rural areas and then enhance the daytime SUHII (Yao et al. 2019; Zhou et al. 2014). Therefore, daytime SUHII was greater in southeastern China and in summer. Comparatively, nighttime SUHII differed more slightly across cities and seasons. This result can be explained by insufficient vegetation transpiration during the nighttime (Yao et al. 2018b; Zhou et al. 2014).
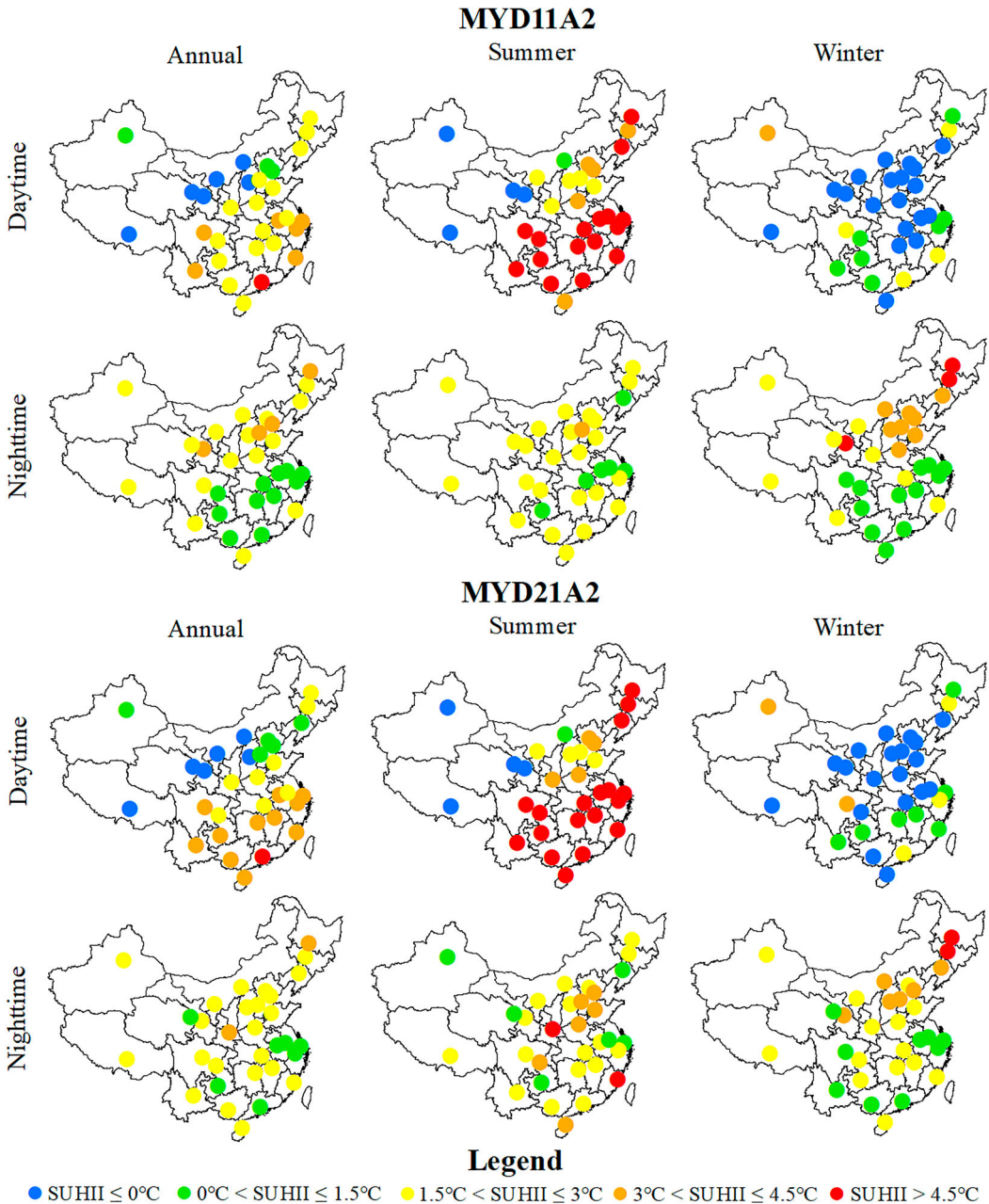

Figure 7. Spatial distribution of surface urban heat island intensity (SUHII) in mainland China in 2015, as revealed by the MYD11A2 and MYD21A2 products.
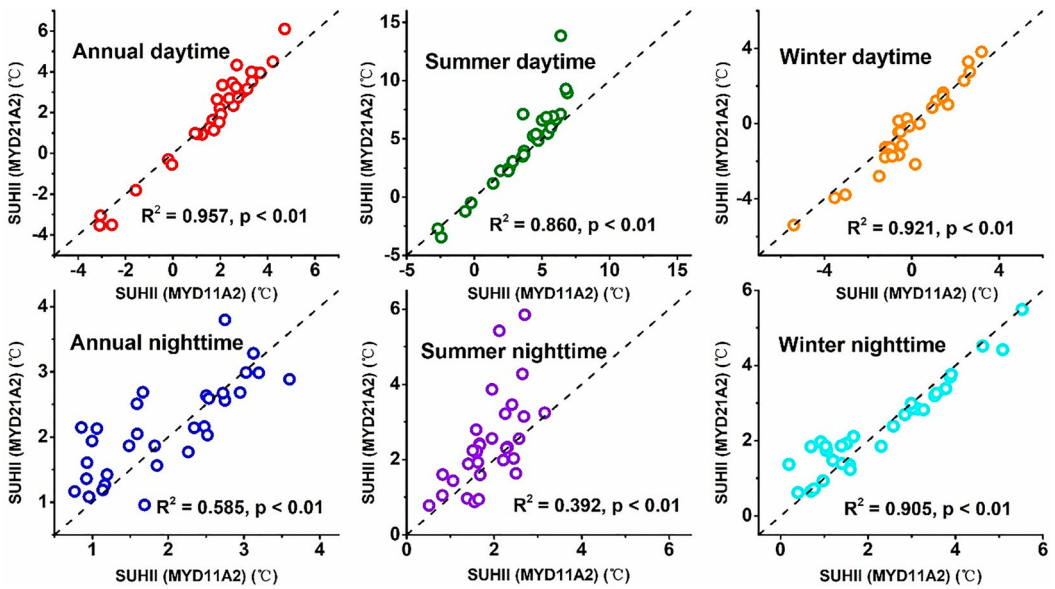
Figure 8. SUHII in 2015 revealed by the MYD11A2 and MYD21A2 products. R^2: coefficient of determination.

The SUHII revealed by the MYD11A2 product was significantly ($p < 0.01$) linked with the MYD21A2 product across 31 cities in mainland China (Figure 8). The coefficients of determination (R^2) were all higher than 0.86 for daytime SUHII. The R^2 values of daytime SUHII were significantly higher than those of nighttime SUHII, which could be attributed to the larger range in daytime SUHII than in nighttime SUHII across cities. Note that some cities had much higher SUHII values revealed by MYD21A2 than by MYD11A2. For example, the daytime SUHII values in summer in Nanning revealed by MYD11A2 and MYD21A2 were 6.87 and 13.85°C, respectively. The nighttime SUHII in summer in Fuzhou was 2.12 and 5.42°C for MYD11A2 and MYD21A2, respectively. These results are because the SUHII revealed by the MYD21A2 product was affected by extremely high LSTs. Although the 8-day composite MYD21A2 product was averaged in summer, there were some pixels with a nighttime LST higher than 50°C in Fuzhou and a daytime LST higher than 100°C in Nanning. The results above clearly indicate that the estimation of SUHII by the MYD21A2 product was significantly affected by outliers. Therefore, caution should be paid when using the MYD21A2 product to analyze SUHII, as well as in other fields. In addition, methods to remove the outliers should be considered in the next version of MxD21 products.

The long-term trends of SUHII (for the period of 2001–2018, calculated using linear regression analysis) revealed by the MYD11A2 product were significantly linked with the MYD21A2 product across 31 major cities, with R^2 values that were all higher than 0.76 and significance level (p) values that were all lower than 0.01 (Figure 9). However, the linear regression slope of SUHII in UAs revealed by MYD21A2 was higher than that revealed by MYD11A2 in most cities. In addition, the slopes of the annual daytime and nighttime SUHII in UAs revealed by the MYD21A2 product, as averaged for 31 cities, were 0.125 and 0.089°C/year, respectively, which were higher than those revealed by the MYD11A2 product (daytime: 0.093°C/year; nighttime: 0.071°C/year). The accuracy of LST retrieval is strongly related to the accuracy of emissivity. The MYD11 product assigned the emissivity according to land cover type using MODIS land cover products (Wan 2013). However, MODIS land cover products were found to be outdated (Chakraborty and Lee 2019; Li et al. 2017; Yao et al. 2017a). For example, Yao et al. (2017a) found that the urban extents in version 5 MCD12Q1 data were nearly the same from 2001 to 2013 in Chinese cities, which have undergone rapid urbanization. Further examination of MYD11A2 emissivity data showed that the emissivity
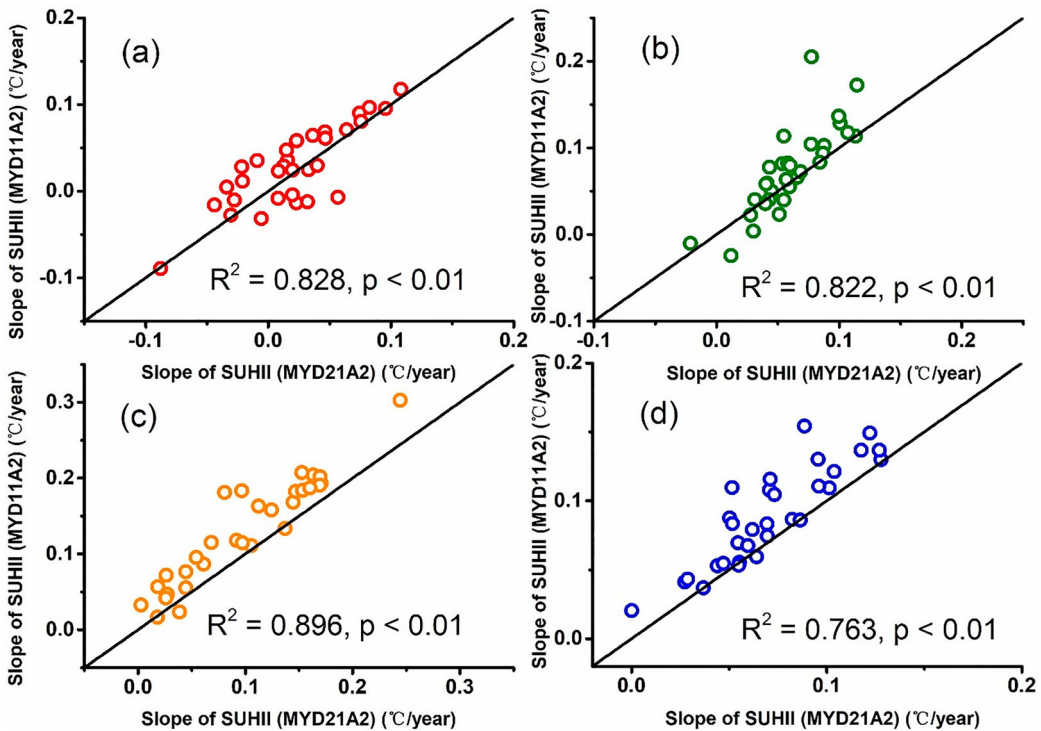
Figure 9. Long-term trends of SUHII from 2003–2018 as revealed by the MYD11A2 and MYD21A2 products: (a) annual daytime SUHII in old urban areas (OUAs); (b) annual nighttime SUHII in OUAs; (c) annual daytime SUHII in urbanizing areas (UAs) and (d) annual nighttime SUHII in UAs.

was significantly lower in urban areas than in rural areas, but the extents of areas with low emissivity were almost unchanged from 2003 to 2018 (Figure 10a and b). Therefore, the assignment of emissivity according to land cover type may lead to errors in LST retrieval in UAs, which further translate into an underestimation of the slope of SUHII in UAs. Previous studies may have slightly underestimated the slope of the long-term SUHII trends because they used MxD11 LST products (Chakraborty and Lee 2019; Peng et al. 2018; Yao et al. 2019; Yao et al. 2017b; Yao et al. 2018b; Zhou et al. 2016). In addition, there were no significant differences in emissivity between urban and rural areas in the MYD21A2 emissivity data (Figure 10c and d). This result suggests that the MYD21 data may have uncertainties when used to study the SUHI effect. Previous studies have validated the MYD21 LST data over bare, vegetated and water sites (Hulley, Malakar, and Freepartner 2016a; Ermida et al. 2014; Coll et al. 2016). The accuracy of the MYD21 LST products over urban sites is still unknown and should be validated in future studies.

4. Conclusions

In this study, a detailed comparison between the MYD11 and MYD21 products was conducted in mainland China. The LST of the MYD21 product was higher than that of the MYD11 product in most areas of China, this could be attributed to the different methods used to retrieve the LST between the two products. The proportions of valid values for MYD21 products were higher than those of the MYD11 products at most regions in China. This result is because these two MODIS LST products use different methods to reduce the effects of clouds. Furthermore, the extremely high LST reached up to 500°C, and the extremely low LST was below −100°C in the MYD21 products. The outliers are less significant in MYD11 because the outliers in the MYD11 are excluded
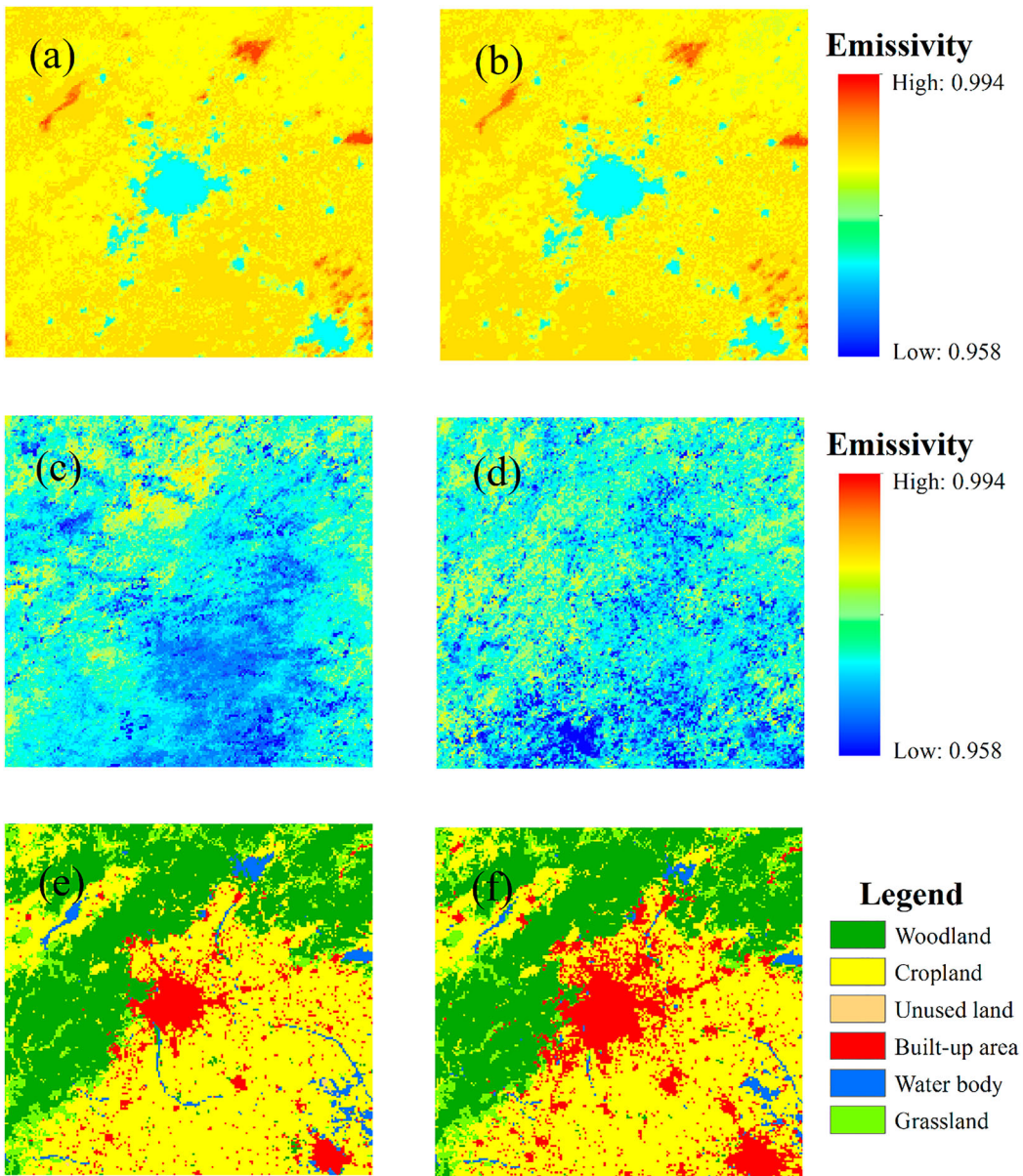
Figure 10. Emissivity and land cover types in Beijing and its surrounding areas. (a) Emissivity of MYD11A2 data in summer 2003. (b) Emissivity of MYD11A2 data in summer 2018. (c) Emissivity of MYD21A2 data in summer 2003. (d) Emissivity of MYD21A2 data in summer 2018. (e) Land cover type in 2000. (f) Land cover type in 2015.

using restrictions on temporal variations in LST. Although the SUHII revealed by MYD11A2 was significantly ($p < 0.01$) correlated with MYD21A2 across 31 major cities in mainland China, outliers in MYD21A2 can result in seasonal average SUHII differences greater than 3°C between MYD11A2 and MYD21A2. Finally, previous studies may have slightly underestimated the slope of the long-term SUHII trends because they used MxD11 LST products. In addition, MYD21 LST and emissivity data may have some uncertainties in urban areas.

Overall, this study showed that MYD21 products had more missing and extreme values compared with MYD11 products. Both MYD11 and MYD21 products have some uncertainties in terms of

studying the SUHI effect. Future studies should compare the two products in other fields (e.g. estimating air temperature and evapotranspiration) and further improve the MODIS LST products.

ORCID

Lunche Wang http://orcid.org/0000-0001-7783-5725

References

Bhattarai, N., K. Mallick, J. Stuart, B. D. Vishwakarma, R. Niraula, S. Sen, and M. Jain. 2019. "An Automated Multi-Model Evapotranspiration Mapping Framework Using Remotely Sensed and Reanalysis Data." *Remote Sensing of Environment* 229: 69–92.

Chakraborty, T., and X. Lee. 2019. "A Simplified Urban-Extent Algorithm to Characterize Surface Urban Heat Islands on a Global Scale and Examine Vegetation Control on their Spatiotemporal Variability." *International Journal of Applied Earth Observation and Geoinformation* 74: 269–280.

Coll, C., V. García-Santos, R. Niclòs, and V. Caselles. 2016. "Test of the MODIS Land Surface Temperature and Emissivity Separation Algorithm With Ground Measurements Over a Rice Paddy." *IEEE Transactions on Geoscience and Remote Sensing* 54: 3061–3069.

Ding, Y., G. Ren, Z. Zhao, Y. Xu, Y. Luo, Q. Li, and J. Zhang. 2007. "Detection, Causes and Projection of Climate Change Over China: An Overview of Recent Progress." *Advances in Atmospheric Sciences* 24: 954–971.

Duan, S.-B., Z.-L. Li, H. Li, F.-M. Göttsche, H. Wu, W. Zhao, P. Leng, X. Zhang, and C. Coll. 2019. "Validation of Collection 6 MODIS Land Surface Temperature Product Using in Situ Measurements." *Remote Sensing of Environment* 225: 16–29.

Duan, S.-B., Z.-L. Li, H. Wu, P. Leng, M. Gao, and C. Wang. 2018. "Radiance-Based Validation of Land Surface Temperature Products Derived from Collection 6 MODIS Thermal Infrared Data." *International Journal of Applied Earth Observation and Geoinformation* 70: 84–92.

Ermida, S. L., I. F. Trigo, C. C. DaCamara, F. M. Göttsche, F. S. Olesen, and G. Hulley. 2014. "Validation of Remotely Sensed Surface Temperature Over an oak Woodland Landscape — The Problem of Viewing and Illumination Geometries." *Remote Sensing of Environment* 148: 16–27.

Han, G., and J. Xu. 2013. "Land Surface Phenology and Land Surface Temperature Changes Along an Urban-Rural Gradient in Yangtze River Delta, China." *Environmental Management* 52: 234–249.

Huang, X., T. Hu, J. Li, Q. Wang, and J. A. Benediktsson. 2018. "Mapping Urban Areas in China Using Multisource Data with a Novel Ensemble SVM Method." *IEEE Transactions on Geoscience and Remote Sensing* 56: 4258–4273.

Hulley, G. 2019. National Aeronautics and Space Administration. Land Surface Temperature/Emissivity (MOD21). https://modis-land.gsfc.nasa.gov/temp21.html.

Hulley, G., R. Freepartner, N. Malakar, and S. Sarkar. 2016b. *Moderate Resolution Imaging Spectroradiometer (MODIS) Land Surface Temperature and Emissivity Product (MxD21) User Guide Collection-6*. Pasadena, California: Jet Propulsion Laboratory, California Institute of Technology.

Hulley, G., N. Malakar, and R. Freepartner. 2016a. *Moderate Resolution Imaging Spectroradiometer (MODIS) Land Surface Temperature and Emissivity Product (MxD21) Algorithm Theoretical Basis Document Collection-6*. Pasadena, California: Jet Propulsion Laboratory, California Institute of Technology.

Hulley, G. C., N. K. Malakar, T. Islam, and R. J. Freepartner. 2018. "NASA's MODIS and VIIRS Land Surface Temperature and Emissivity Products: A Long-Term and Consistent Earth System Data Record." *IEEE Journal of Selected Topics in Applied Earth Observations and Remote Sensing* 11: 522–535.

Hulley, G., S. Veraverbeke, and S. Hook. 2014. "Thermal-Based Techniques for Land Cover Change Detection Using a new Dynamic MODIS Multispectral Emissivity Product (MOD21)." *Remote Sensing of Environment* 140: 755–765.

Islam, T., G. C. Hulley, N. K. Malakar, R. G. Radocinski, P. C. Guillevic, and S. J. Hook. 2017. "A Physics-Based Algorithm for the Simultaneous Retrieval of Land Surface Temperature and Emissivity From VIIRS Thermal Infrared Data." *IEEE Transactions on Geoscience and Remote Sensing* 55: 563–576.

Kuang, W., J. Liu, J. Dong, W. Chi, and C. Zhang. 2016. "The Rapid and Massive Urban and Industrial Land Expansions in China Between 1990 and 2010: A CLUD-Based Analysis of Their Trajectories, Patterns, and Drivers." *Landscape and Urban Planning* 145: 21–33.

Li, X., J. P. Messina, N. J. Moore, P. Fan, and A. M. Shortridge. 2017. "MODIS Land Cover Uncertainty in Regional Climate Simulations." *Climate Dynamics* 49: 4047–4059.

Liu, J., W. Kuang, Z. Zhang, X. Xu, Y. Qin, J. Ning, J. Zhou, et al. 2014. "Spatiotemporal Characteristics, Patterns, and Causes of Land-use Changes in China Since the Late 1980s." *Journal of Geographical Sciences* 24: 195–210.

Lu, N., S. Liang, G. Huang, J. Qin, L. Yao, D. Wang, and K. Yang. 2018. "Hierarchical Bayesian Space-Time Estimation of Monthly Maximum and Minimum Surface air Temperature." *Remote Sensing of Environment* 211: 48–58.

Malakar, N. K., and G. C. Hulley. 2016. "A Water Vapor Scaling Model for Improved Land Surface Temperature and Emissivity Separation of MODIS Thermal Infrared Data." *Remote Sensing of Environment* 182: 252–264.

MODIS Reprojection Tool V4.1 Software. Accessed January 31, 2016. https://lpdaac.usgs.gov/lpdaac/tools/modis_reprojection_tool.

Niu, Z., L. Wang, L. Fang, J. Li, and R. Yao. 2019. "Analysis of Spatiotemporal Variability in Temperature Extremes in the Yellow and Yangtze River Basins During 1961–2014 Based on High-Density Gauge Observations." *International Journal of Climatology*. doi:10.1002/joc.6188.

Peng, J., J. Ma, Q. Liu, Y. Liu, Y. Hu, Y. Li, and Y. Yue. 2018. "Spatial-Temporal Change of Land Surface Temperature Across 285 Cities in China: An Urban-Rural Contrast Perspective." *Science of The Total Environment* 635: 487–497.

Phan, T. N., and M. Kappas. 2018. "Application of MODIS Land Surface Temperature Data: A Systematic Literature Review and Analysis." *Journal of Applied Remote Sensing* 12: 1.

Wan, Z. 1999. *MODIS Land-Surface Temperature Algorithm Theoretical Basis Document (LST ATBD)*. Santa Barbara: Institute for Computational Earth System Science.

Wan, Z. 2008. "New Refinements and Validation of the MODIS Land-Surface Temperature/Emissivity Products." *Remote Sensing of Environment* 112: 59–74.

Wan, Z. 2013. *Collection-6 MODIS Land Surface Temperature Products Users' Guide. ERI*. Santa Barbara: University of California.

Wan, Z. 2014. "New Refinements and Validation of the Collection-6 MODIS Land-Surface Temperature/Emissivity Product." *Remote Sensing of Environment* 140: 36–45.

Wan, Z., and J. Dozier. 1996. "A Generalized Split-Window Algorithm for Retrieving Land-Surface Temperature from Space." *IEEE Transactions on Geoscience and Remote Sensing* 34: 892–905.

Wei, J., W. Huang, Z. Li, W. Xue, Y. Peng, L. Sun, and M. Cribb. 2019a. "Estimating 1-km-Resolution $PM_{2.5}$ Concentrations Across China Using the Space-Time Random Forest Approach." *Remote Sensing of Environment* 231: 111221. doi:10.1016/j.rse.2019.111221.

Wei, J., Z. Li, J. Guo, L. Sun, W. Huang, W. Xue, T. Fan, and M. Cribb. 2019b. "Satellite-derived 1-km-Resolution PM_1 Concentrations from 2014 to 2018 Across China." *Environmental Science & Technology* 53 (22): 13265–13274.

Weng, Q. 2009. "Thermal Infrared Remote Sensing for Urban Climate and Environmental Studies: Methods, Applications, and Trends." *ISPRS Journal of Photogrammetry and Remote Sensing* 64: 335–344.

Wu, X., G. Wang, R. Yao, L. Wang, D. Yu, and X. Gui. 2019. "Investigating Surface Urban Heat Islands in South America Based on MODIS Data from 2003–2016." *Remote Sensing* 11: 1212.

Xu, Y., A. Knudby, Y. Shen, and Y. Liu. 2018. "Mapping Monthly Air Temperature in the Tibetan Plateau From MODIS Data Based on Machine Learning Methods." *IEEE Journal of Selected Topics in Applied Earth Observations and Remote Sensing* 11: 345–354.

Xu, K., B. Xu, J. Ju, C. Wu, H. Dai, and B. X. Hu. 2019. "Projection and Uncertainty of Precipitation Extremes in the CMIP5 Multimodel Ensembles Over Nine Major Basins in China." *Atmospheric Research* 226: 122–137.

Yao, R., L. Wang, X. Gui, Y. Zheng, H. Zhang, and X. Huang. 2017a. "Urbanization Effects on Vegetation and Surface Urban Heat Islands in China's Yangtze River Basin." *Remote Sensing* 9: 540.

Yao, R., L. Wang, X. Huang, J. Chen, J. Li, and Z. Niu. 2018a. "Less Sensitive of Urban Surface to Climate Variability Than Rural in Northern China." *Science of The Total Environment* 628–629: 650–660.

Yao, R., L. Wang, X. Huang, W. Gong, and X. Xia. 2019. "Greening in Rural Areas Increases the Surface Urban Heat Island Intensity." *Geophysical Research Letters* 46: 2204–2212.

Yao, R., L. Wang, X. Huang, Z. Niu, F. Liu, and Q. Wang. 2017b. "Temporal Trends of Surface Urban Heat Islands and Associated Determinants in Major Chinese Cities." *Science of The Total Environment* 609: 742–754.

Yao, R., L. Wang, X. Huang, W. Zhang, J. Li, and Z. Niu. 2018b. "Interannual Variations in Surface Urban Heat Island Intensity and Associated Drivers in China." *Journal of Environmental Management* 222: 86–94.

Zhang, X., M. A. Friedl, C. B. Schaaf, A. H. Strahler, and A. Schneider. 2004. "The Footprint of Urban Climates on Vegetation Phenology." *Geophysical Research Letters* 31, n/a–n/a.

Zhou, C., and K. Wang. 2016. "Land Surface Temperature Over Global Deserts: Means, Variability, and Trends." *Journal of Geophysical Research: Atmospheres* 121: 14344–14357.

Zhou, D., J. Xiao, S. Bonafoni, C. Berger, K. Deilami, Y. Zhou, S. Frolking, R. Yao, Z. Qiao, and J. Sobrino. 2018. "Satellite Remote Sensing of Surface Urban Heat Islands: Progress, Challenges, and Perspectives." *Remote Sensing* 11: 48.

Zhou, D., L. Zhang, L. Hao, G. Sun, Y. Liu, and C. Zhu. 2016. "Spatiotemporal Trends of Urban Heat Island Effect Along the Urban Development Intensity Gradient in China." *Science of The Total Environment* 544: 617–626.

Zhou, D., S. Zhao, S. Liu, L. Zhang, and C. Zhu. 2014. "Surface Urban Heat Island in China's 32 Major Cities: Spatial Patterns and Drivers." *Remote Sensing of Environment* 152: 51–61.

Zhou, D., S. Zhao, L. Zhang, G. Sun, and Y. Liu. 2015. "The Footprint of Urban Heat Island Effect in China." *Scientific Reports* 5: 11160.